

















ORIGINAL RESEARCH

In Vivo Magnetic Resonance Imaging-Based Detection of Heterogeneous Endothelial Response in Thoracic and Abdominal Aorta to Short-Term High-Fat Diet Ascribed to Differences in Perivascular Adipose Tissue in Mice

Anna Bar , PhD; Anna Kieronska-Rudek , MSc; Bartosz Proniewski , PhD; Joanna Suraj-Prażmowska , PhD; Krzysztof Czamara , PhD; Brygida Marczyk , MSc; Karolina Matyjaszczyk-Gwarda , PhD; Agnieszka Jaształ , MSc; Edyta Kuś , PhD; Zuzanna Majka , MSc; Agnieszka Kaczor , PhD; Anna Kurpińska , PhD; Maria Walczak , PhD; Elsbet J. Pieterman , B.Sc; Hans M. G. Princen , PhD; Stefan Chlopicki , MD, PhD

BACKGROUND: Long-term feeding with a high-fat diet (HFD) induces endothelial dysfunction in mice, but early HFD-induced effects on endothelium have not been well characterized.

METHODS AND RESULTS: Using an magnetic resonance imaging-based methodology that allows characterization of endothelial function in vivo, we demonstrated that short-term (2 weeks) feeding with a HFD to *C57BL/6* mice or to *E3L.CETP* mice resulted in the impairment of acetylcholine-induced response in the abdominal aorta (AA), whereas, in the thoracic aorta (TA), the acetylcholine-induced response was largely preserved. Similarly, HFD resulted in arterial stiffness in the AA, but not in the TA. The difference in HFD-induced response was ascribed to distinct characteristics of perivascular adipose tissue in the TA and AA, related to brown- and white-like adipose tissue, respectively, as assessed by histology, immunohistochemistry, and Raman spectroscopy. In contrast, short-term HFD-induced endothelial dysfunction could not be linked to systemic insulin resistance, changes in plasma concentration of nitrite, or concentration of biomarkers of glycocalyx disruption (syndecan-1 and endocan), endothelial inflammation (soluble form of vascular cell adhesion molecule 1, soluble form of intercellular adhesion molecule 1 and soluble form of E-selectin), endothelial permeability (soluble form of fms-like tyrosine kinase 1 and angiotensin II), and hemostasis (tissue plasminogen activator and plasminogen activator inhibitor 1).

CONCLUSIONS: Short-term feeding with a HFD induces endothelial dysfunction in the AA but not in the TA, which could be ascribed to a differential response of perivascular adipose tissue to a HFD in the AA versus TA. Importantly, early endothelial dysfunction in the AA is not linked to elevation of classical systemic biomarkers of endothelial dysfunction.

Key Words: endothelial function ■ high-fat diet-fed mice ■ magnetic resonance imaging ■ perivascular adipose tissue ■ thoracic and abdominal aorta

Correspondence to: Stefan Chlopicki, MD, PhD, Jagiellonian Centre for Experimental Therapeutics (JCET), Jagiellonian University, ul. Bobrzynskiego 14, 30-348 Krakow, Poland. E-mail: stefan.chlopicki@jcet.eu

Supplementary Material for this article is available at <https://www.ahajournals.org/doi/suppl/10.1161/JAHA.120.016929>

For Sources of Funding and Disclosures, see page 15.

© 2020 The Authors. Published on behalf of the American Heart Association, Inc., by Wiley. This is an open access article under the terms of the Creative Commons Attribution-NonCommercial License, which permits use, distribution and reproduction in any medium, provided the original work is properly cited and is not used for commercial purposes.

JAHA is available at: www.ahajournals.org/journal/jaha

CLINICAL PERSPECTIVE

What Is New?

- In the present study, using state-of-the-art magnetic resonance imaging-based assessment of endothelial response in vivo in vessels with intact perivascular adipose tissue, we demonstrated distinct effects of a high-fat diet on endothelial phenotype in the thoracic and abdominal aorta in mice.
- The results show that even a short-term (2 weeks) feeding with a high-fat diet results in severe endothelial dysfunction in the abdominal aorta, whereas endothelial function in the thoracic aorta is resistant to early high-fat diet-induced dysfunction. This difference was ascribed to distinct perivascular adipose tissue composition, with white adipose tissue-like characteristics in the abdominal aorta and brown adipose tissue-like characteristics in the thoracic aorta.

What Are the Clinical Implications?

- Early endothelial dysfunction induced by fat load was also described in humans. Our results show that perivascular adipose tissue depots determine endothelial response to a high-fat diet promoting or preventing endothelial dysfunction even after short-term feeding; therefore, perivascular adipose tissue plays a key role in the regulation of endothelial function and represents an important target for diagnosis and vasoprotective therapy to be explored clinically.

Phospho-eNOS	phosphorylated endothelial NO synthase
PVAT	perivascular adipose tissue
PWV	pulse wave velocity
UCP-1	uncoupling protein 1
TA	thoracic aorta

Endothelial dysfunction is a hallmark of various diseases including metabolic syndrome,¹ and the assessment of NO-dependent vasodilation in the coronary or peripheral circulation predicts adverse cardiovascular events and poor long-term outcomes.^{2,3}

In experimental conditions, in various models of endothelial dysfunction, endothelium-dependent function in large and small vessels is classically studied in the myograph setups,^{4–6} and perivascular adipose tissue (PVAT) is usually removed for studies in isolated aorta preparation, even though this tissue has a well-documented influence on endothelial function.⁷

Indeed, PVAT plays an important role in the regulation of vascular function.^{8,9} Under physiological conditions, PVAT releases a number of adipokines, such as adipocyte-derived relaxing factor,¹⁰ which have a beneficial anticontractile effect on vascular function and are essential for the maintenance of vascular homeostasis.¹¹ Accumulation of PVAT, e.g., in obesity,^{12,13} was associated with impaired anticontractile function as well as perivascular inflammation.^{14,15}

Altogether, there is increasing experimental evidence to suggest that both structural and functional alterations in PVAT, in obesity and metabolic syndrome, might contribute to endothelial dysfunction, increasing the risk for atherosclerosis and hypertension development.^{15,16} Furthermore, there are numerous reports describing long-term effects (>8 weeks) of high-fat diet (HFD) feeding on endothelial function in mice.^{17–21} However, to the best of our knowledge, there are no reports that have characterized the effects of short-term HFD feeding on endothelial function, taking into account heterogeneous characteristics of PVAT in various parts of the aorta and their distinct sensitivity to HFD-induced inflammation.^{7,22,23}

Regional differences in PVAT even within different regions of the same vessel, e.g., in the aorta, were reported.⁷ In rodents, fat surrounding the thoracic aorta (TA) has brown adipose tissue-like characteristics, whereas periaortic fat in the abdominal aorta (AA) has similar features to white adipose tissue.^{7,24} Generally, brown PVAT shows resistance to HFD-induced inflammation in the perivascular tissue²² in contrast to white PVAT, which is highly responsive to HFD with marked increases in macrophage infiltration and cytokine expression,²³ leading to increases in oxidative stress.¹⁴

Nonstandard Abbreviations and Acronyms

3D	3-dimensional
AA	abdominal aorta
Ach	acetylcholine
DETC	diethyldithiocarbamic acid sodium salt
E3L.CETP	APOE*3-Leiden.human Cholesteryl Ester Transfer Protein transgenic mice
EPR	electron paramagnetic resonance
eWAT	epididymal white adipose tissue
GTT	glucose tolerance test
HFD	high-fat diet
iBAT	interscapular brown adipose tissue

However, it is not known whether regional differences of PVAT in the aorta between AA and TA influence development of endothelial dysfunction in the early phase of HFD.

Accordingly, the aim of the present study was to characterize a possibly distinct response of endothelium in the AA and TA in relation to PVAT characteristics (assessed by histology, immunohistochemistry, and Raman spectroscopy) after short-term (2, 4, and 8 weeks) feeding with a HFD in mice. To assess endothelial function *in vivo*, we used a 3-dimensional (3D) magnetic resonance imaging (MRI)-based method.²⁵ This methodology does not have the limitations of *ex vivo* vascular studies and allows study of endothelial function *in vivo* in the presence of intact PVAT surrounding the studied vessel. To determine whether systemic effects of short-term HFD feeding might account for the observed differences in endothelium-dependent vasodilation in the TA and AA, we comprehensively assessed the systemic response to short-term HFD feeding by measuring insulin resistance, plasma concentrations of nitrite and nitrate, oxidative stress in red blood cells, and plasma concentration of various biomarkers of endothelial dysfunction.²⁶

METHODS

The data, analytic methods, and study materials will be made available on request to other researchers for purposes of reproducing the results or replicating the procedures.

Animals

Studies were performed in 6-week-old *C57BL/6* male mice (from Mossakowski Medical Research Centre, Polish Academy of Sciences, Warsaw, Poland), fed a HFD (HFD_{60%}, 60 kcal% of fat +1% of cholesterol; ZooLab, Krakow, Poland) for 2, 4, and 8 weeks (measurements at 8, 10, and 14 weeks of age, respectively) in comparison to age-matched *C57BL/6* male mice fed a control diet (AIN93G, ZooLab). Moreover, to confirm that regional differences in endothelial response in the aorta in response to a HFD can also be observed as early as after 2 weeks in another murine model, we chose APOE*3-Leiden. human Cholesteryl Ester Transfer Protein transgenic (*E3L.CETP*) mice (from the Netherlands Organisation for Applied Scientific Research, Metabolic Health Research, Leiden, Netherlands), an established and well-recognized model for hyperlipidemia and atherosclerosis.^{27,28} The study was performed on 12-week-old female *E3L.CETP* mice, at the stage before the development of endothelial dysfunction (A. Bar, PhD, unpublished results, 2020). *E3L.CETP* mice were

fed a HFD containing cacao butter (HFD_{32%}, 15% cacao butter (32 kcal%)+1% cholesterol, Charles River Laboratories) for 2 weeks (measurements at 14 weeks of age) and 16 weeks (only glucose tolerance test [GTT] at 28 weeks of age) in comparison to age-matched *C57BL/6J* female mice (from Charles River Laboratories) fed a control diet (standard diet, Altromin, AnimaLab). The experiment involved 16 to 18 mice per group in most of the end point measurements but in some assessments (e.g., MRI measurements) in which the biggest differences were expected in readouts, a lower number of animals (from 5 to 8) was used. The size of a given experimental group is reported in the legends of the corresponding graphs. Mice were housed in collective cages, in a room with constant environmental conditions (22–25°C, 65%–75% humidity, and 12-hour light/dark cycle) and were weighed at the beginning and after 2, 4, and 8 weeks of feeding, presented as percentage weight changes after respective diet duration. Animals had *ad libitum* access to daily provided diets and water. All experiments were approved by the local ethics committee of Jagiellonian University (Krakow, Poland, identification code: 82/2016 date of approval: May 31, 2016) and were in accordance with the *Guide for the Care and Use of Laboratory Animals* of the National Academy of Sciences (National Institutes of Health publication No. 85–23, revised 1996), as well as the Guidelines for Animal Care and Treatment of the European Community.

Assessment of Insulin Resistance Based on GTT

Before GTT was performed, mice were fasted for 4 hours with access to water. Baseline glucose level was measured using a standard glucometer in a drop of blood from the tail, cut at the end. Blood glucose concentration measurements were repeated after 15, 30, 45, 60, and 120 minutes of intraperitoneal glucose administration (2 g/kg body weight). Results are presented as a curve of blood glucose concentration in time and as an area under the curve.

Assessment of Acetylcholine-Induced Vasodilation *In Vivo* by MRI

MRI experiments were performed using a 9.4 T scanner (BioSpec 94/20, USR). During the MRI experiment, mice were anaesthetized using isoflurane (Aerrane, Baxter Sp. z o. o., 1.5 vol%) in oxygen and air (1:2) mixture and imaged in the supine position. Heart function (rhythm and ECG), respiration, and body temperature (maintained at 37°C using circulating warm water) were monitored using a Monitoring and Gating System (SA Instruments, Inc.).

Endothelial function *in vivo* was assessed by a previously described technique^{25,29,30} as an endothelium-dependent response to acetylcholine (ACh) administration. Response to injection of ACh (Sigma-Aldrich; 50 μ L, 16.6 mg/kg, IP; dose of ACh was based on a previous study²⁵) was analyzed in the AA and TA.

Vasomotor responses were examined by comparing 2, time-resolved 3D images of the vessels before and 25 minutes after intraperitoneal ACh administration. The optimal time to measure ACh-induced vasorelaxation was chosen based on our previous work.²⁵ 3D images of the aorta were acquired using the cine IntraGate FLASH 3D sequence and reconstructed with the IntraGate 1.2.b.2 macro (Bruker). Analysis was performed using ImageJ software 1.46r (National Institutes of Health) and scripts written in MATLAB (MathWorks), in the hyperstack of the AA (10 slices in diastole, from the renal arteries down) and the TA (10 slices in diastole, from the celiac artery up). All cross-sectional areas of vessels at each slice were obtained using thresholding segmentation and exported to MATLAB, where vessel volumes were reconstructed and calculated.

Imaging parameters included the following: repetition time—6.4 ms, echo time—1.4 ms, field of view—30 \times 30 \times 14 mm³ for aorta, matrix size—256 \times 256 \times 35, flip angle—30°, and number of accumulations—15, reconstructed to 7 cardiac frames. Total scan time was about 12 minutes.

Assessment of Aortic Pulse Wave Velocity

Pulse wave velocity (PWV) measurements were performed using a Doppler flow velocity system (Indus Instruments, Scintica Instrumentation).³¹ During Doppler measurements, mice were anaesthetized using isoflurane (Aerrane; Baxter Sp. z o. o., 1.5 vol%) oxygen and air (1:2), mixture. Mice were taped supine to ECG electrodes incorporated into a temperature-controlled printed circuit board. The temperature of each mouse was monitored with a rectal probe and body temperature was maintained at 37°C. Before measurements, the chest and right hind limb of the mice were shaved.

The PWV, an index of arterial stiffness,³² was measured using two 20-MHz Doppler probes, by simultaneously recording velocity signals from 2 sites, representative for the TA and AA. The TA measurements were performed by measuring velocities in the aortic arch and in the descending aorta about 15 to 20 mm distal to the first probe. To obtain a signal from the descending aorta, the probe was placed just under the sternum and angled toward the heart at a depth of 4 mm. Measurements in the TA were performed by placing the second probe tip at the

base of the left upper limb, oriented almost parallel to the board surface and aimed toward the upper mid-chest at a depth of 6 mm. The AA measurements were performed by measuring the velocities in the descending aorta and \approx 25 to 30 mm distal to the first probe in the right femoral artery by placing the second probe on the right hind limb of the mice and angled toward the murine groin at a depth of 3 to 4 mm. Aortic PWV was calculated by dividing the separation distance by the difference in arrival times of the velocity pulse timed with respect to the ECG.³¹ Signal analysis was performed using Doppler signal processing workstation (version 1.625, Indus Instruments).

Blood Sampling and Tissue Collection

At the end of the experiment, mice were anaesthetized (100 mg/kg ketamine+10 mg/kg xylazine, IP) and blood was drawn from the heart and collected in tubes containing 10% solution of ethylenediaminetetraacetic acid dipotassium salt (Aqua-Med; 1 μ L of EDTA/100 μ L of blood). Next, blood was mixed with MS-SAFE Protease and Phosphatase Inhibitor (Sigma-Aldrich) in a ratio of 100:1. All samples were centrifuged at 664g, at a temperature of 4°C for 10 minutes to isolate plasma, as previously described.²⁶ Obtained plasma samples were deep-frozen at -80°C for high-performance liquid chromatography measurements of nitrate (NO_3^-) and nitrite (NO_2^-) concentrations by ENO-20 NOx Analyser as well as for microLC/MS-MRM measurements of biomarkers of endothelial dysfunction. The remaining blood was deep-frozen at -80°C for measurements of glutathione concentration in red blood cells as described below. Aorta, PVAT, and liver were collected for further *ex vivo* assessments as described below. Moreover, liver, as well as perirenal adipose tissue and epididymal adipose tissue, were weighted after collection.

Histological Assessment of Liver Steatosis

Liver sections were stained with Oil Red O for lipids visualization, and at least 9 images of each liver were randomly obtained under \times 200 magnification. In detail, the image segmentation was performed using simple intensity thresholding. First, the source image was thresholded to extract the tissue image from the background, next within the tissue area another thresholding step was performed to obtain red, Oil Red O-stained lipids droplets mask. Finally, the area of the background, tissue, and lipid droplets were calculated. Liver steatosis was expressed as the percentage of fat area versus tissue area, calculated in the left liver lobe, using the Columbus Image Data

Storage and Analysis System (PerkinElmer) with an algorithm adapted for quantitative analysis of Oil Red O–stained sections. Similar results were obtained after calculation of oil area versus background image area in the left liver lobe, as well as in the entire tissue of the liver. Therefore, other parameters were not presented.

Characteristic of PVAT of the TA and AA by Immunohistochemistry

Formalin-fixed and paraffin-embedded thoracic and abdominal parts of the aorta with PVAT were cut into 5- μ m slices. Antigen retrieval was performed according to the standard protocol. Area of the brown and white adipose tissue in PVAT was assessed by double staining using perilipin and UCP-1 (uncoupling protein 1) antibodies. To visualize the total PVAT area, a perilipin antibody (primary anti-perilipin-1 antibody, ab61682) was used, whereas the area of brown adipose tissue was identified by UCP-1 staining (primary anti-UCP-1 antibody, ab209483). Sections were incubated with the secondary antibodies FITC-conjugated donkey anti-goat IgG (705-454-003) and Cy3-conjugated donkey anti-rabbit (711-165-152). To characterize the functional differences between brown and white adipose tissue, the lectin I and phosphorylated endothelial NO synthase (Phospho-eNOS) were stained. To visualize glyco-calyx of microvessels in PVAT, biotinylated Lectin I (B-1105) was used. Phospho-eNOS—Ser1177 (9571) (primary Phospho-eNOS [Ser1177] antibody, #9571) was used to detect inflammatory processes in endothelium. Then, sections were incubated with the secondary antibody biotinylated-conjugated goat anti-rabbit IgG (111-065-003). Then the slices were incubated with VECTASTAIN Elite ABC-HRP Kit and diaminobenzidine (Sigma) to obtain the colour reaction. Subsequently, the cross-sections of the TAs and AAs with PVAT were photographed ($\times 100$ magnification) and images were acquired using an AxioCam MRc5 digital camera and an AxioObserver 22 D1 inverted fluorescent microscope (Zeiss) or BX51 microscope (Olympus). Before analysis in the pictures with Lectin I and Phospho-eNOS nonadipose tissue (aorta, muscles, lymph nodes) fragments were manually excised. Image segmentation was performed using Ilastik (developed by the Ilastik team, with partial financial support of the Heidelberg Collaboratory for Image Processing, HHMI Janelia Farm Research Campus and CellNetworks Excellence Cluster). The pixels corresponding to the UCP-1 immunopositive area, as well as perilipin immunopositive area (FITC channel), were quantitatively determined using ImageJ software 1.46r as demonstrated in Figure S1. The mean number of pixels representing UCP-1 and

perilipin were counted using ImageJ software. The results were expressed as the ratio of brown adipose tissue area (number of UCP-1 immunopositive pixels/PVAT area), area of microvessels (number of Lectin I immunopositive pixels/PVAT area), or activated endothelium (Phospho-eNOS immunopositive pixels/PVAT area) and normalized to the respective control.

Characteristic of PVAT of the TA and AA by Raman Spectroscopy

Samples of the interscapular brown adipose tissue (iBAT), epididymal white adipose tissue (eWAT; from the adipose tissue attached to the epididymis and testicle), and PVATs of the TA and AA were isolated from wild-type C57BL/6J male mice fed an AIN93G or HFD for 4 weeks. Periaortic PVAT samples of the TA and AA were extracted from the descending aorta distal to the aortic arch and from the part of the artery lying in the abdominal cavity, respectively. For Raman spectroscopic measurements, all samples were rinsed in NaCl isotonic solution to wash traces of blood and put onto CaF₂ slides as previously described.³³

The Raman spectra of the iBAT, eWAT, and PVAT samples were acquired using a confocal WITec Alpha300 Raman spectrometer (WITec) equipped with a 532-nm laser, 20 \times air objective (Nikon S Plan Fluor, numerical aperture=0.45), UHTS 300 spectrograph (600 grooves-mm⁻¹ grating), and CCD detector (Andor, DU401A-BV-352). For each sample, at least 5 single Raman spectra were collected using the maximum laser power at the sample position (≈ 28 mW). The single spectra of 32 accumulations and the integration time of 0.5 second were normalized in the 1800 to 400 cm⁻¹ spectral range and averaged over all mice for each studied adipose tissue type.

All Raman spectra underwent routine preprocessing including baseline correction using an autopolynomial of degree 3 and an automatic cosmic ray removal procedure. Preprocessing was performed using the WITec Project Plus software. Raman spectra were averaged per type of adipose tissue and presented using the OriginPro 9.1 program. The OPUS 7.2 program was used for calculations of the integral intensity (I) of the bands at ca. 1660 and 1445 cm⁻¹, enabling estimation of the lipid unsaturation degree (I1660/I1445). The results were tested by ANOVA performed using Prism software (GraphPad Software, Inc.) to characterize the differences in unsaturation of lipids in various types of the adipose tissue in a quantitative manner.

Assessment of Endothelial NO Production in the Aorta Using Electron Paramagnetic Resonance

For measurements of eNOS-dependent NO production, electron paramagnetic resonance (EPR)

spin-trapping with diethyldithiocarbamic acid sodium salt (DETC) was used *ex vivo*, as previously described,³⁴ with minor modifications. The isolated aorta was divided into 2 parts: the abdominal and thoracic sections. Only half of the group of samples of the AA and TA were cleared from surrounding tissue, and the other half were analyzed in the presence of PVAT. Parts of the aorta were opened longitudinally and preincubated with 10 $\mu\text{mol/L}$ of N6-(1-Iminoethyl)-lysine, hydrochloride (L-NIL) in Krebs-HEPES buffer for 30 minutes at 37°C. Addition of L-NIL during the preincubation period allowed the direct measurements of NO produced by eNOS without the signal from NO produced by inducible NO synthase expressed by macrophages in atherosclerotic plaque,³⁵ as previously described.^{30,34,36} Next, DETC (3.6 mg) and $\text{FeSO}_4 \cdot 7\text{H}_2\text{O}$ (2.25 mg) were separately dissolved under argon gas bubbling in two 10-mL volumes of ice-cold Krebs-Hepes buffer and were kept under gas flow on ice until use. After preincubation, a spin trap (125 μL of $\text{FeSO}_4 \cdot 7\text{H}_2\text{O}$ and 125 μL of DETC—final concentration of the colloid: 285 $\mu\text{mol/L}$) and calcium ionophore A23187 (the final concentration: 1 $\mu\text{mol/L}$) were added to the parts of aorta. Subsequently, incubation for 90 minutes at 37°C was started. Finally, dried aorta was weighed and frozen in liquid nitrogen (suspended in fresh buffer) into the middle of a 400- μL column of Krebs-Hepes buffer and stored at -80°C until measured. EPR spectra were obtained using an X-band EPR spectrometer (EMX Plus), equipped with a rectangular resonator cavity H102. Signals were quantified by measuring the total amplitude of the NO-Fe(DETC)_2 after correction of baseline. The quantitative results of NO production assessed by EPR were expressed in AU/mg of tissue and normalized to the respective controls.

Assessment of Reduced Glutathione and Oxidized Glutathione in Red Blood Cells by Capillary Electrophoresis

A P/ACE MDQ capillary electrophoresis system (Beckman Coulter) with 32 Karat software (version 8.0, Beckman Coulter) was used for analyses. The apparatus was equipped with a PDA detector set at 200 nm. Separation of the analytes took place in an uncoated fused-silica capillary (60.2 cm total length, 50 cm effective length, 50 μm ID, and 375 μm OD) thermostated at 25°C with a constant voltage of 25 kV ($\approx 6.5 \mu\text{A}$). BisTRIS (75 mmol/L), boric acid (25 mmol/L) buffer adjusted to pH 7.8 by adding 1 mol/L NaOH, was chosen as a background electrolyte. Samples were introduced to the capillary by hydrodynamic injection for 20 seconds by 3.5 kPa, followed by injection of ultrapure H_2O for 2 seconds by 3.5 kPa. Between

analytical runs, the capillary was rinsed with 1 mol/L of NaOH, ultrapure water, and background electrolyte, respectively (138 kPa; 2 minutes each). Obtained data were analyzed by PeakFit software (version 4.12, Systat Software).

Measurements of reduced glutathione and oxidized glutathione were performed as described by Hempe et al.³⁷ Briefly, red blood cells were first separated from plasma by centrifuging whole blood. A hemolysate was prepared by adding to 50 μL of red blood cells, 200 μL of hemolyzing reagent (10 mmol/L KCN and 5 mmol/L EDTA in ultrapure H_2O). Then, samples were deproteinated by adding 100 μL of 5% metaphosphoric acid to 100 μL of hemolysate. After centrifugation (10 000g for 10 minutes at 4°C), the metaphosphoric acid extracts were diluted 1:4 with ultrapure H_2O and then used for capillary electrophoresis analysis. All chemicals except boric acid (J.T. Baker) and NaOH (VWR International) were purchased from Sigma-Aldrich.

Assessment of Biomarkers of Endothelial Dysfunction in Plasma by MicroLC/MS-MRM

Assessment of 10 protein biomarkers of endothelial dysfunction was performed using a microLC/MS-MRM method as previously described.^{26,30,38–40} The panel included biomarkers of various aspects of endothelial dysfunction such as glycocalyx disruption: syndecan-1 and endocan; endothelial inflammation: soluble form of vascular cell adhesion molecule 1, soluble form of E-selectin and soluble form of intercellular adhesion molecule 1; endothelial permeability: angiopoietin 2 and soluble form of fms-like tyrosine kinase 1; and hemostasis: von Willebrand factor, tissue plasminogen activator and plasminogen activator inhibitor 1.

A UPLC Nexera system (Shimadzu) connected to a highly sensitive mass spectrometer QTrap 5500 (Sciex) was used. During sample preparation, the murine plasma was subjected to proteolytic digestion using porcine trypsin to achieve unique and reproducible peptide sequences, applied as the surrogates of the proteins suitable for LC-MS/MS analyses. A detailed description of the targeted analysis of a selected panel of proteins was presented elsewhere.^{26,38,39}

Statistical Analysis

The study included separated mice groups to collect organs and tissue for further analysis after 2, 4, and 8 weeks of HFD feeding. Data are presented as mean and SD or in the case of a lack of normal distribution (Shapiro-Wilk test), as median and interquartile range. Statistical tests were performed using GraphPad Prism. Nonparametric (Kruskal-Wallis test

or Mann–Whitney *U* test) or parametric (1- and 2-way ANOVA with Tukey test, repeated measures ANOVA, unpaired *t* Student test) tests were performed. A value of $P \leq 0.05$ was considered to be statistically significant.

RESULTS

General Characteristics of C57BL/6 Mice Fed a HFD (HFD_{60%}) for 2 to 8 Weeks

Effects of feeding with an HFD_{60%} were manifested by insulin resistance, as evidenced by an increased level of blood glucose concentration in GTT. In C57BL/6 mice fed an HFD_{60%} for only 2 weeks, the area under the GTT curve was significantly increased (area under the curve ≈ 2 -fold higher in C57BL/6 mice fed a HFD_{60%}, in comparison to C57BL/6 mice fed a standard diet), and was maintained at a similar level after 4 and 8 weeks of HFD_{60%} feeding (Figure 1B).

HFD_{60%} also induced mild liver steatosis that was similar after 2, 4, and 8 weeks of HFD_{60%} (in a range between 9.1% and 14.7% as compared with 1.0% in mice fed a standard diet; Figure 1E). Early liver steatosis was not associated with changes in body weight (Figure 1A), liver mass (liver mass ≈ 1.0 g in all experimental groups), or changes in the mass of epididymal (Figure 1C) and perirenal (Figure 1D) adipose tissue. However, after 4 and 8 weeks of an HFD_{60%}, the masses of epididymal adipose tissue and perirenal adipose tissue were ≈ 2 - and 3-fold higher, respectively, and body weight also changed (by 20% in comparison to mice fed a standard diet).

Early Impairment of Acetylcholine-Induced Vasodilation and NO Production in the AA But Not in the TA in C57BL/6 Mice Fed HFD (HFD_{60%})—the Relationship With PVAT Characteristics

After 2 weeks' feeding of C57BL/6 mice with an HFD_{60%}, impairment of Ach-induced vasodilation in the AA (Figure 2B) was observed as paradoxical vasoconstriction (volume changes of the AA: -27.8% in comparison to 13.7% in age-matched control mice) with progression of endothelial dysfunction in HFD_{60%} mice after 4 and 8 weeks of HFD_{60%} feeding. In contrast, Ach-induced vasodilation in the TA was fully preserved throughout the 2- to 8-week period of HFD_{60%} feeding (Figure 2A).

Moreover, 4 to 8 weeks of feeding with HFD_{60%} induced arterial stiffness as evidenced by an increased value of the PWV in the AA (≈ 1.5 -fold increase of PWV in comparison to control mice, Figure S2B), which was not observed in the TA (Figure S2A).

Differential response to HFD_{60%} of the AA and TA was also confirmed by EPR measurements of NO production in aorta ex vivo (Figure 3A through 3D). In aorta with preserved PVAT, NO production level was maintained in the TA (Figure 3A) and decreased ($\approx 30\%$) in the AA (Figure 3B) in HFD_{60%}-fed mice in comparison to control mice. Furthermore, impaired NO production in the aorta with and without PVAT was observed in the AA (Figure 3D) but not in the TA (Figure 3C).

The difference in the AA and TA response to a short period of HFD_{60%} was associated with distinct characteristics of PVAT in the TA and AA, related to brown and white adipose tissue, respectively. In fact, 2 weeks of HFD_{60%} feeding induced a nonsignificant fall ($P=0.2$) in the amount of brown adipose tissue in the AA, which was even more pronounced and significant (≈ 2.5 -fold decrease of brown adipose tissue amount) after 4 to 8 weeks of HFD_{60%} ($P=0.02$ and $P=0.03$, respectively) (Figure 2D and 2F), whereas in the TA, HFD_{60%} feeding did not induce any significant changes in the amount of brown fat tissue in PVAT (Figure 2C and 2E) after 2, 4, or 8 weeks of HFD feeding. Furthermore, 2 weeks of HFD_{60%} feeding induced a significant increase in the lectin (Figure S3A and S3B) and a decrease in the Phospho-eNOS (Figure S3C and S3D) contents in PVAT of the aorta, with the latter change more pronounced in the AA (lectin: 12% higher, Phospho-eNOS: 11% lower in comparison to control mice; Figure S3B and S3D) than in the TA (lectin: 6% higher, Phospho-eNOS: 7% lower in comparison to control mice; Figure S3A and S3C), although the observed difference was not statistically significant.

To confirm AA and TA differential response to HFD_{60%}, the lipid unsaturation degree was estimated by Raman spectroscopy in PVAT of the TA (Figure S4A) and AA (Figure S4B) in mice after 4 weeks of HFD_{60%} feeding and compared with this parameter for the iBAT (Figure S4C) and eWAT (Figure S4D). HFD_{60%} feeding induced a statistically significant (14%) decrease in lipid unsaturation in the PVAT of the AA that was qualitatively similar to a reduction of lipid unsaturation in the white adipose tissue in eWAT (20%). The decrease of lipid unsaturation was manifested as a decreased intensity of Raman bands at 1660 and 1268 cm^{-1} assigned to the C=C stretching and =C–H deformation vibrations, respectively, and increased intensity of the band at 1445 cm^{-1} , attributable to the CH bending vibrations.⁴¹ Thus, the ratio of the integral intensities of bands at 1660 and 1445 cm^{-1} was chosen to assess the lipid unsaturation as shown in Figure S3. In contrast to the AA and eWAT, HFD_{60%} feeding did not influence lipid unsaturation in the PVAT of TA, nor in the iBAT brown adipose tissue.

Collectively, the Raman spectroscopy measurements showed similar biochemical response in PVAT in the AA and in white adipose tissue and

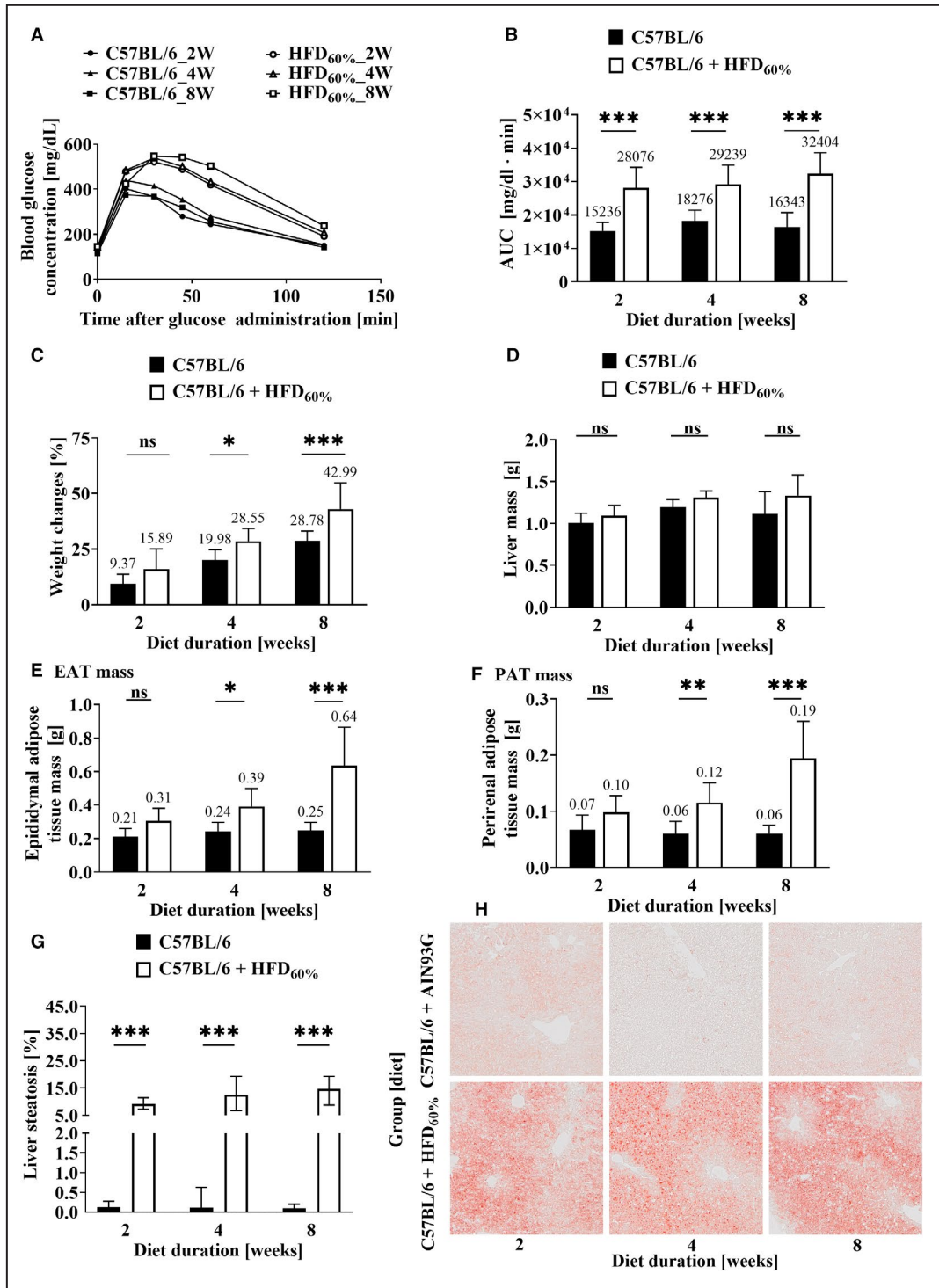


Figure 1. Effects of high-fat diet (HFD; HFD_{60%}) feeding on weight of mice, insulin resistance, epididymal and perirenal adipose tissue, and liver steatosis.

Changes in mice weight (A, $\text{Weight}_{\text{End}} - \text{Weight}_{\text{Start}} / \text{Weight}_{\text{Start}}$), area under the glucose tolerance test (GTT) curve (B), mass of epididymal adipose tissue (EAT mass, C), and perirenal adipose tissue (PAT mass, D) as well as representative images of liver steatosis (E) in C57BL/6 mice fed an HFD (HFD_{60%}, white columns) for 2 (n=16, A through C; n=15, D), 4 (n=16), and 8 (n=18) weeks in comparison to age-matched C57BL/6 mice fed a control diet (black columns, after 2 [n=16, A through C; n=15, D], 4 [n=16], and 8 [n=16, B through D; n=15, A] weeks of feeding). Statistics: 2-way ANOVA followed by Tukey post hoc test (normality was assessed using the Shapiro-Wilk test): not statistically significant (ns) * $P < 0.05$, ** $P < 0.01$, *** $P < 0.001$. AUC indicates area under the curve.

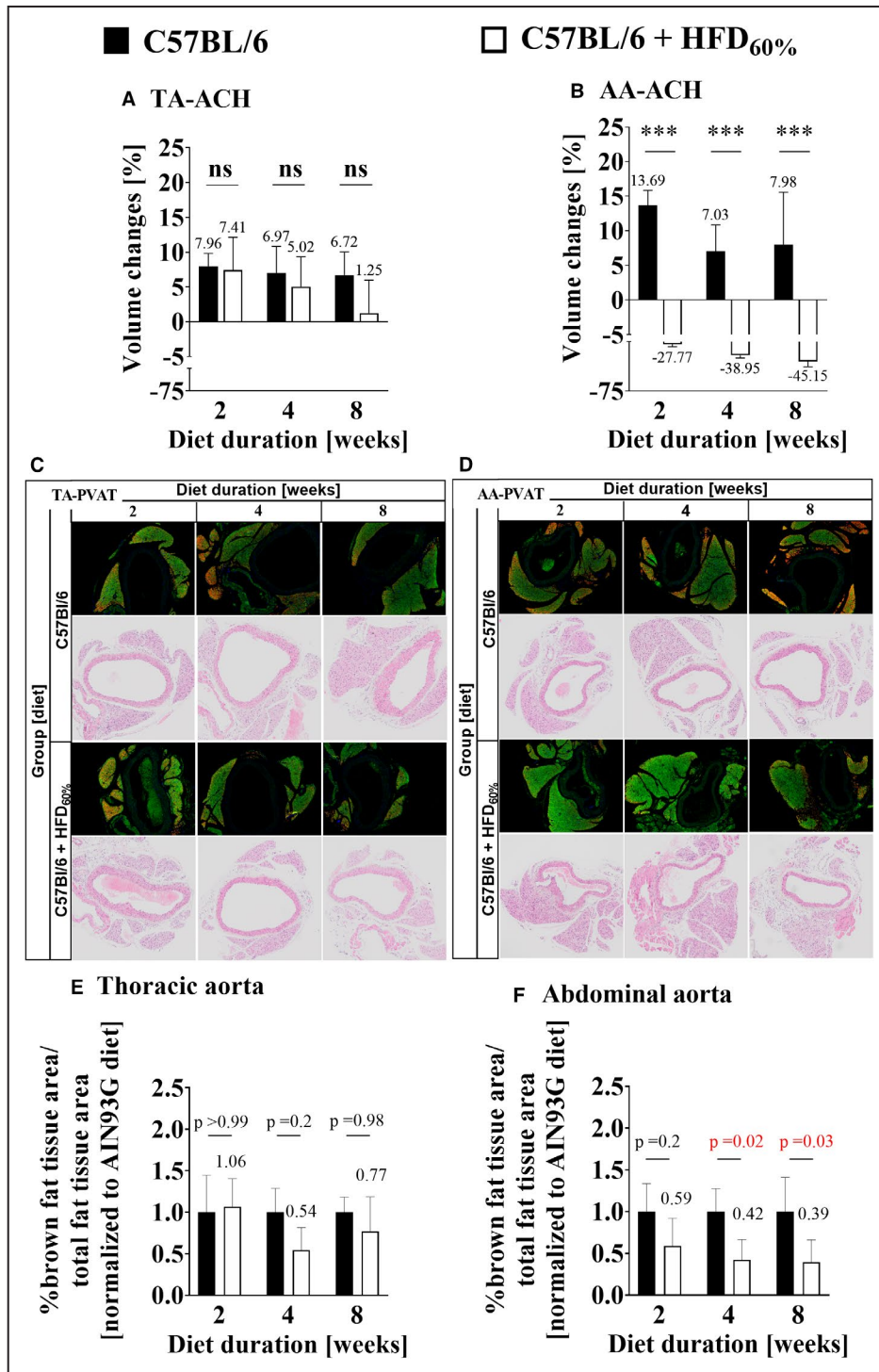


Figure 2. High-fat-diet (HFD; HFD_{60%}) feeding reduces endothelial function in the abdominal aorta (AA) in association with decreased brown fat in perivascular adipose tissue. Changes in end-diastolic volume of the thoracic aorta (TA; **A**, TA-Ach) and AA (**B**, AA-Ach) 25 minutes after acetylcholine (Ach) administration and ratio of brown adipose tissue area to total adipose tissue area as well as representative images of perivascular adipose tissue (PVAT) in the TA (**C** and **E**) and the AA (**D** and **F**) in C57BL/6 mice fed an HFD (HFD_{60%}, white columns) for 2 (n=6, **E** and **F**; n=5, **A** and **B**), 4 (n=6, **A** and **E**; n=5, **B** and **F**), and 8 (n=7, **B**; n=6, **A**; n=5, **E** and **F**) weeks in comparison to age-matched C57BL/6 mice fed a control diet (black columns, after 2 [n=7, **B**; n=6, **A**; n=5, **E**, and **F**], 4 [n=6, **A** and **B**; n=5, **E** and **F**], and 8 [n=8, **F**; n=7, **E**; n=6, **A** and **B**] weeks of feeding). Statistics: 2-way ANOVA followed by Tukey post hoc test (normality was assessed using the Shapiro–Wilk test): not statistically significant (ns), ***P<0.001.

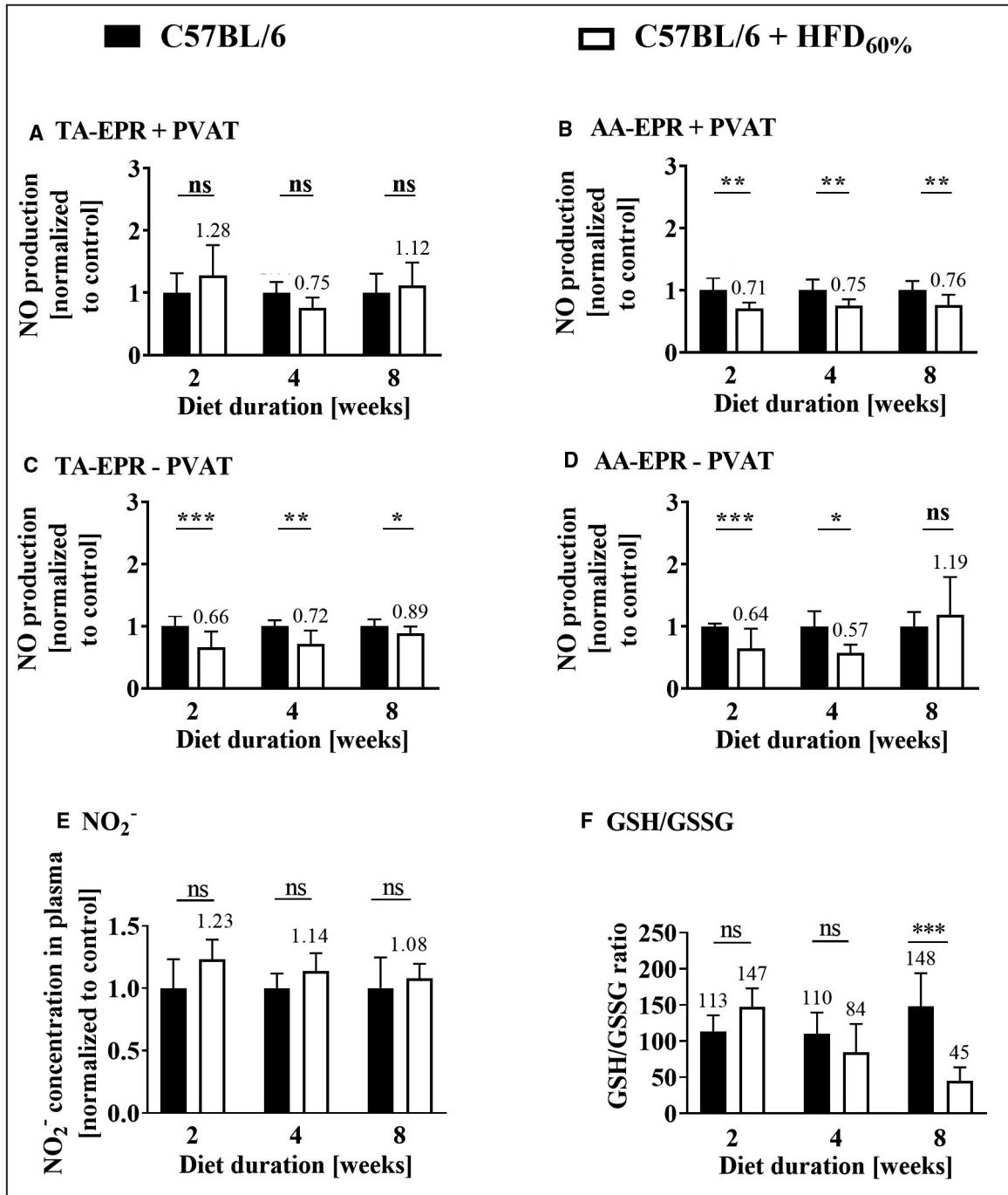


Figure 3. Effects of high-fat diet (HFD; HFD_{60%}) feeding on NO production in the aorta, nitrite concentration in plasma, and level of reduced glutathione (GSH) and oxidized glutathione (GSSG) in red blood cells.

Changes in NO production in the thoracic aorta (TA; **A** and **C**) and the abdominal aorta (AA; **B** and **D**), cleared (**C** and **D**) or not (**A** and **B**) from surrounding adipose tissue, measured by spin-trapping with DETC (sodium diethyldithiocarbamate, spin trap), changes in nitrite (E, NO₂⁻) concentration in plasma, and ratio of GSH and GSSG in red blood cells (**F**, GSH/GSSG) in C57BL/6 mice fed an HFD (HFD_{60%}, white columns) for 2 (n=16, **E**; n=13, **F**; n=8, **A** and **B**; n=7, **C** and **D**), 4 (n=16, **E**; n=15, **F**; n=8, **A** through **D**), and 8 (n=19, **E**; n=18, **F**; n=9, **A**, **B**, and **D**; n=8, **C**) weeks in comparison to age-matched C57BL/6 mice fed a control diet (black columns, after 2 [n=16, **E** and **F**; n=8, **A** and **B**; n=7, **D**; n=6, **C**], 4 [n=16, **E**; n=15, **F**; n=8, **A** through **D**], and 8 [n=16, **E**; n=15, **F**; n=9, **C**; n=8, **D**; n=7, **A** and **B**] weeks of feeding). Statistics: 2-way ANOVA followed by Tukey post hoc test (normality was assessed using the Shapiro–Wilk test): not statistically significant (ns) *P<0.05, **P<0.01, ***P<0.001. EPR indicates electron paramagnetic resonance; and PVAT, perivascular adipose tissue.

similar response in PVAT of the TA and in brown adipose tissue. These results suggest a relative increase in saturated fatty acids in PVAT surrounding the AA, which did not occur in PVAT adjacent to the TA.

Lack of Early Changes in Plasma Concentration of Nitrite and Nitrate and of Biomarkers of Endothelial Dysfunction in C57BL/6 Mice Fed a HFD (HFD_{60%})

Feeding of C57BL/6 mice with a HFD from 2 to 8 weeks did not affect NO₂⁻ (Figure 3E) and NO₃⁻ concentration in plasma (average NO₃⁻ plasma concentration, throughout diet duration in C57BL/6 control mice: 36.1±7.7 μmol/L and HFD_{60%} fed C57BL/6 mice: 35.9±10.7 μmol/L), whereas a change in reduced glutathione/oxidized glutathione ratio (≈a 3-fold decrease in comparison to mice fed a standard diet; Figure 3F) was only seen after 8 weeks of HFD_{60%} feeding. Moreover, with the exception of increased plasma concentration of von Willebrand factor (concentration increased on average by ≈25%, in comparison to mice fed a standard diet, Figure 4H), there were no significant changes in plasma concentration of biomarkers of glycocalyx disruption (syndecan-1 and endocan; Figure 4A and 4B), endothelial inflammation (soluble form of vascular cell adhesion molecule 1, soluble form of intercellular adhesion molecule 1 and E-selectin; Figure 4C through 4E), endothelial permeability (soluble form of fms-like tyrosine kinase 1 and angiopoietin 2; Figure 4F and 4G), and hemostasis (tissue plasminogen activator and plasminogen activator inhibitor 1; Figure 4I and 4J) in HFD_{60%}-fed mice as compared with mice fed a control diet.

Therefore, biomarkers of endothelial function were not sensitive to detect endothelial dysfunction after short-term HFD_{60%} feeding in contrast to the assessment of functional endothelial response measured in vivo.

Early Impairment of Acetylcholine-Induced Vasodilation in the AA But Not in the TA in E3L.CETP Mice Fed a HFD (HFD_{32%})

To confirm that regional differences in the early endothelial response in the AA and the TA to HFD is not limited to one murine model we also studied E3L.CETP mice. Similarly to HFD_{60%} feeding in C57BL/6 mice, 2 weeks of feeding with HFD_{32%} in E3L.CETP mice resulted in paradoxical vasoconstriction in the AA induced by Ach (Figure 5D volume changes of the AA: -4.2% in comparison to 5.3% in age-matched control

mice). However, Ach-induced vasodilation in the TA was fully preserved (Figure 5C).

HFD_{32%} did not induce significant insulin resistance after short-term feeding (area under the curve: ≈1.8-fold higher in E3L.CETP mice fed with HFD_{32%} only after 16 weeks of feeding, in comparison to C57BL/6J mice fed standard diet; Figure 5A). Moreover, 2 weeks of HFD_{32%} feeding was not associated with the changes in body weight in the E3L.CETP mice (Figure 5B) and did not affect NO₂⁻ (Figure 5E) and NO₃⁻ (Figure 5F) concentration in plasma.

Altogether, in E3L.CETP mice fed a HFD_{32%}, even though insulin resistance was not present, the impairment of endothelial function in the AA (but not in the TA) was clearly observed.

DISCUSSION

Using an MRI-based methodology to assess endothelial function in vivo,²⁵ in vessels with intact PVAT, to the best of our knowledge, we demonstrated for the first time, that short-term feeding with a HFD resulted in endothelial dysfunction in the AA, whereas endothelial function in the TA was resistant to early HFD-induced dysfunction. These changes were independently observed in 2 different murine models, C57BL/6 and E3L.CETP mice, fed a HFD of different composition, and were thereby independent of systemic insulin resistance. Endothelial dysfunction in HFD-fed mice for 2 weeks was not associated with systemic changes in NO bioavailability and changes in reduced glutathione/oxidized glutathione ratio in red blood cells as the latter was only observed after 8 weeks of HFD_{60%} feeding, supporting an increase in systemic oxidative stress after 8 weeks but not after 2 weeks of HFD feeding. Furthermore, the concentration of biomarkers of glycocalyx disruption (syndecan-1 and endocan), endothelial inflammation (soluble form of vascular cell adhesion molecule 1, soluble form of intercellular adhesion molecule 1 and E-selectin), endothelial permeability (soluble form of fms-like tyrosine kinase 1 and angiopoietin 2), and hemostasis (tissue plasminogen activator and plasminogen activator inhibitor 1) were not significantly altered. In contrast, these biomarkers changed typically in other models of endothelial dysfunction in our previous studies.^{30,39,42} The heterogeneous endothelial response in the abdominal and thoracic parts of the aorta in response to short-term feeding with a HFD was ascribed to a distinct difference in the composition of white- and brown-like adipose tissue of PVAT in the AA and TA, as assessed by histology, immunohistochemistry, and Raman spectroscopy. Furthermore, the different endothelial response in the AA versus TA was mirrored

by deterioration of arterial stiffness in the AA but not in the TA, underscoring the distinct functional consequences of PVAT-modulated endothelial response for the entire vascular wall. Altogether, our results support the notion of the important role of PVAT in the early phase of HFD-induced vascular dysfunction operating in some but not in all vessels that could not be detected on the basis of classical systemic biomarkers of endothelial dysfunction. These results underscore the insidious nature of early endothelial dysfunction in response to fat overload.

To assess endothelial function in vivo, in vessels with intact PVAT, a 3D MRI-based methodology was used. This methodology is well suited for detection and quantification, with good sensitivity and reproducibility, of NO-dependent endothelial response, and has been previously used to characterize endothelial function in the different murine models in vivo.^{25,29,30,43}

In the present study, we focused on the short-term effects of a HFD, in particular after a 2-week period of HFD in *C57BL/6* mice, a model that is characterized by the early development of insulin resistance and liver steatosis. The salient finding of this study was the detection of severe endothelial dysfunction after only 2 weeks of HFD_{60%} feeding, as evidenced by a substantial impairment of Ach-induced vasodilation in the AA, which was reverted to vasoconstriction, the magnitude of which was even more pronounced as compared with previously studied 28-week-old ApoE/*LDLR*^{-/-} mice with advanced atherosclerosis.³⁰

Our in vivo MRI-based approach revealed the robust impairment of endothelial function in the AA (but not in the TA) after 2 weeks of feeding with a HFD, which was barely detectable using ex vivo settings in previous work even after 4 weeks of a HFD,^{44,45} but was clearly present after 16 to 20 weeks of a HFD^{17,21} or an even longer feeding (eg, 8 months²⁰). Indeed, previously, only a marginal effect was seen in isolated aorta ex vivo after a short period of 4 weeks of HFD feeding in the magnitude of Ach-induced vasodilation, insulin-dependent vasodilation, or magnitude of phenylephrine-induced vasoconstriction.^{44–46}

We also demonstrated that HFD-induced endothelial dysfunction progressed into the development of arterial stiffness, which was observed as increased PWV in the AA after 4 to 8 weeks but not after 2 weeks of

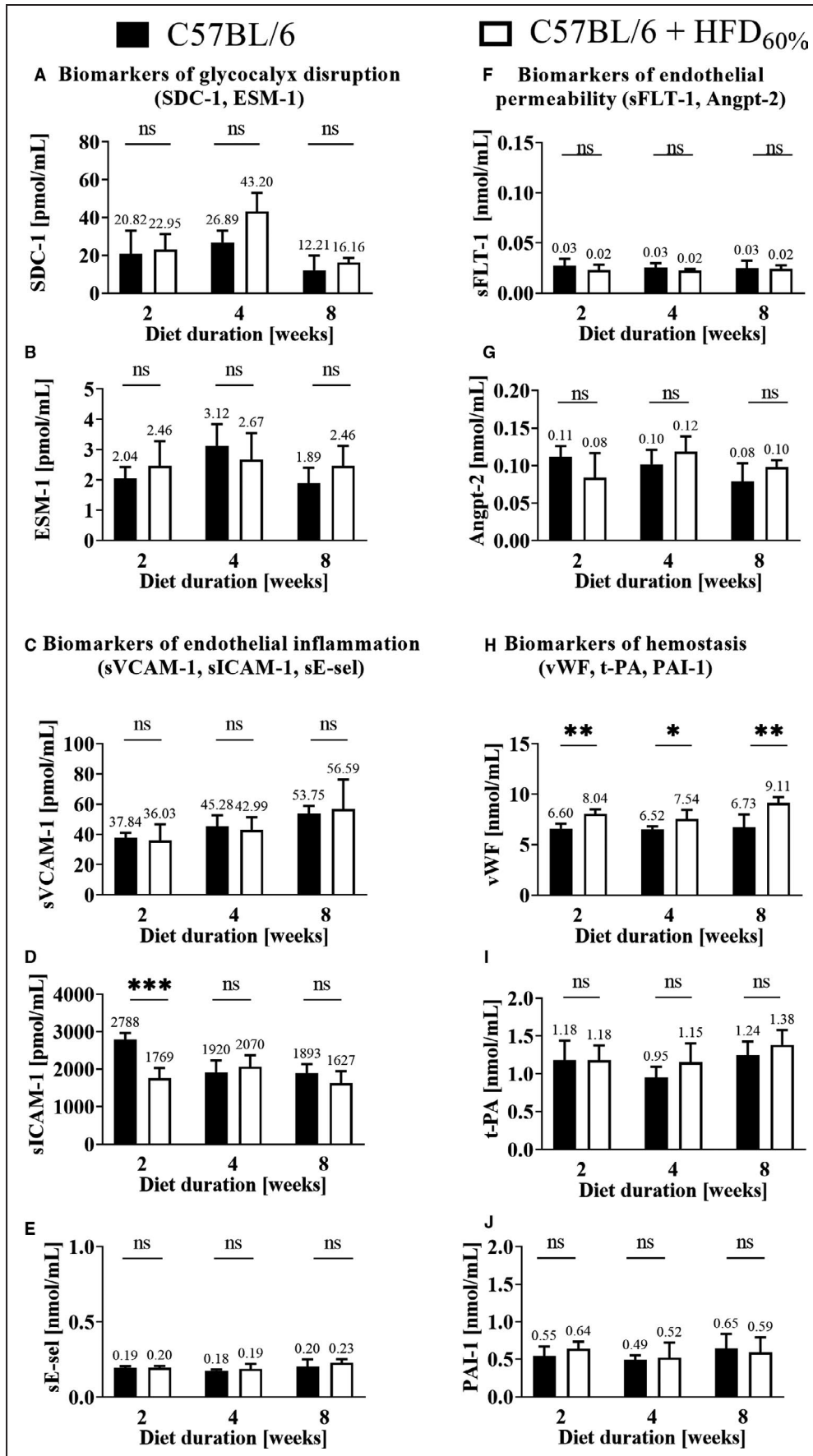
HFD feeding. Arterial stiffness of the TA did not change, again underscoring the regional differences between the AA and TA in response to a short-term HFD.

In addition to the assessment of PVAT characteristics in the AA and TA by histology and immunohistochemistry, Raman spectroscopy revealed that PVAT in the AA and TA displayed a different profile of lipid unsaturation, showing striking similarities between PVAT in the AA and eWAT as well as between PVAT in the TA and iBAT. These observations confirm the notion that PVAT in the AA and TA shows a predominantly white and brown phenotype, respectively, in line with our previous report using Raman spectroscopy-based assessment of PVAT in the aorta in ageing mice⁴¹ and with other studies showing distinct characteristics of PVAT in the TA and the AA in mice.^{7,22,24,47} Most importantly, a significant decrease of lipid unsaturation in PVAT of AA (and eWAT) was observed in response to HFD_{60%} feeding, whereas PVAT of TA (and iBAT) was resistant to the increased amount of saturated lipids in the diet. The heterogeneous response of the AA and TA was also observed in EPR measurements in the ex vivo aorta, suggesting that the vasoprotective activity of PVAT was lost in the AA but not in the TA. Altogether, our results reveal that these 2 distinct PVAT depots have essentially antagonistic functions on endothelial function in the aorta in response to an HFD that either promote or prevent endothelial dysfunction in the AA and TA, respectively.

It should be underlined that there is not a clear division in pure brown adipose tissue or pure white adipose tissue between these 2 PVATs because infiltrations of one type of PVAT can be found in the other.⁷ White adipose tissue, which is composed of adipocytes with a large, single fat droplet, is presumed to be the main depot for lipid storage also in perivascular tissue⁴⁸ that is highly responsive to HFD.²³ Conversely, brown PVAT, which contains several smaller fat droplets and numerous mitochondria, displays vasoprotective activity,²² participates in the regulation of intravascular temperature⁴⁹ and shows resistance to a HFD; thus, it protects the vascular wall against diet-induced inflammation, as well as against atherosclerosis.^{22,49}

To confirm that heterogeneous early effects of HFD feeding on endothelium in the TA and AA could be detected by MRI in vivo in another model as well,

Figure 4. Effects of high-fat diet (HFD; HFD_{60%}) feeding on plasma concentration of protein biomarkers of endothelial dysfunction. Concentrations of syndecan-1 (SDC-1) (A), endocan (ESM-1) (B), soluble form of vascular cell adhesion molecule 1 (sVCAM-1) (C), soluble form of intercellular adhesion molecule 1 (sICAM-1) (D), soluble form of E-selectin (sE-sel) (E), soluble form of fms-like tyrosine kinase 1 (sFLT-1) (F), angiopoietin 2 (Angpt-2) (G), von Willebrand factor (vWF) (H), tissue plasminogen activator (t-PA) (I), and plasminogen activator inhibitor 1 (PAI-1) (J) in plasma, in *C57BL/6* mice fed a HFD (HFD_{60%} white columns) for 2 (n=16, C through J; n=15, A and B), 4 (n=16, A through G, I, and J; n=14, H), and 8 (n=19, B, and D through J; n=18, A and C) weeks in comparison to age-matched *C57BL/6* mice fed a control diet (black columns, after 2 [n=16, B, H, and I; n=15, D; n=12, C, E through G, and J; n=11, A], 4 [n=16, A through G, I, and J; n=15, H], and 8 [n=16, B, D, G through I; n=15, A, C, E, F, and J] weeks of feeding). Statistics: B and I, 2-way ANOVA followed by Tukey post hoc test (A, C through H, and J); Kruskal–Wallis ANOVA (normality was assessed using the Shapiro–Wilk test): not statistically significant (ns) **P*<0.05, ***P*<0.01, ****P*<0.001.



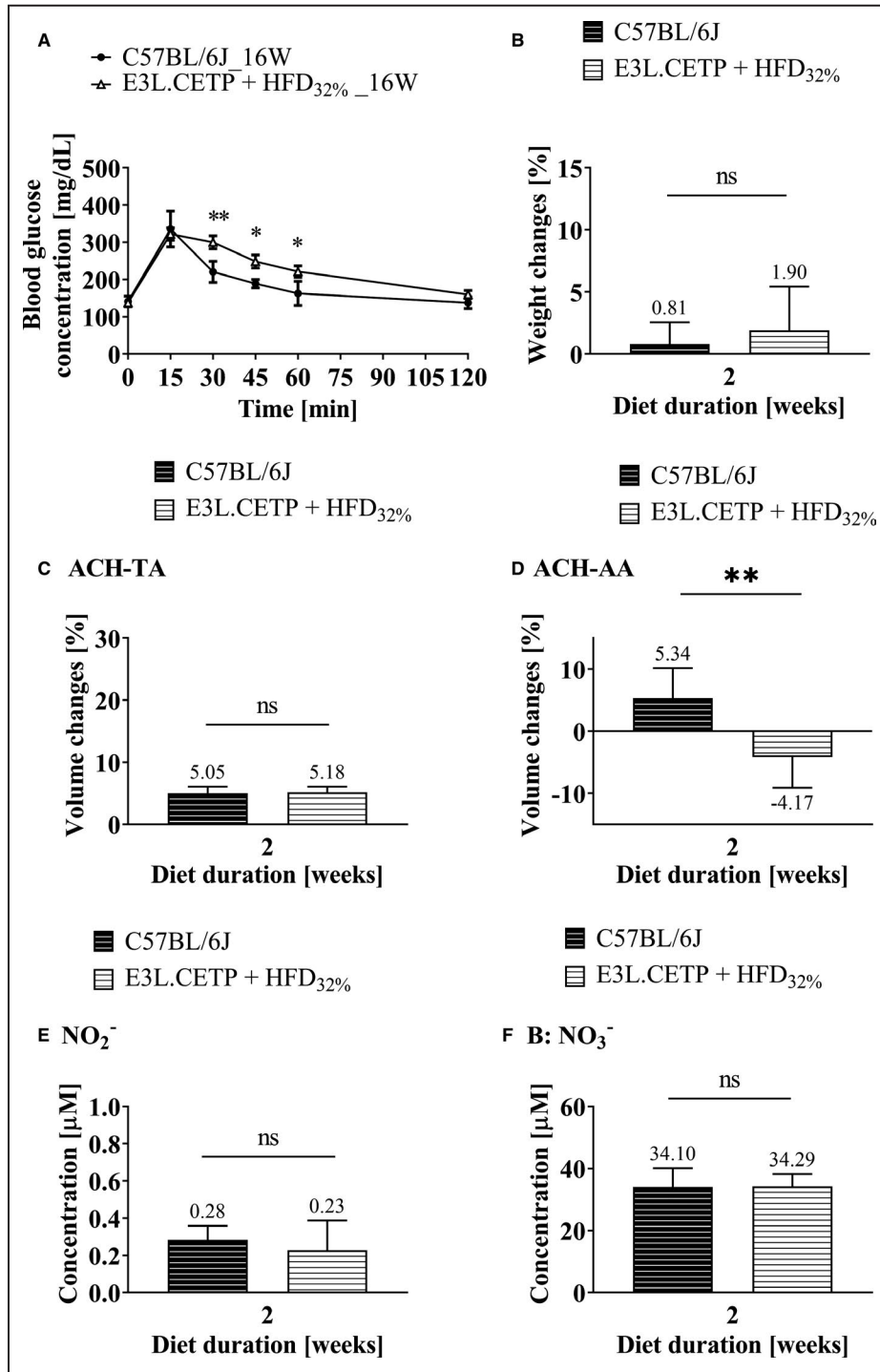


Figure 5. Effects of high-fat diet (HFD; HFD_{32%}) feeding on insulin resistance, weight of the mice, endothelial function, and nitrite and nitrate concentration in plasma in E3L.CETP mice. Blood glucose concentration 0, 15, 30, 45, 60, and 120 minutes after glucose administration (A), changes in mouse weight (B, $\text{Weight}_{\text{End}} - \text{Weight}_{\text{Start}} / \text{Weight}_{\text{Start}}$), changes in end-diastolic volume of the thoracic aorta (TA; C, TA-Ach), and abdominal aorta (AA; D, AA-Ach) 25 minutes after acetylcholine (Ach) administration as well as changes in nitrite (E: NO₂⁻) and nitrate (F: NO₃⁻) concentration in plasma in E3L.CETP mice fed a HFD (HFD_{32%}; white columns with horizontal lines or triangles) for 2 (B through F) and 16 (A) weeks (n=8) in comparison to age-matched C57BL/6J mice fed a standard diet (black columns with horizontal lines or circles, n=6, A, B, E, and F; n=5, C and D). Statistics: (A): repeated measures ANOVA, (B, E, and F): Mann-Whitney U test, (C and D): Student t test (normality was assessed using the Shapiro-Wilk test): not statistically significant (ns) *P<0.05, **P<0.01, .

we used a murine model for hyperlipidemia and atherosclerosis (*E3L.CETP* mice^{27,28}), which is based on the introduction of 3 human genes: apolipoprotein E*3 Leiden, apolipoprotein C1, and CETP.^{27,50} These mice exhibit a human-like lipoprotein metabolism⁵¹ and respond similarly to humans to pharmacological interventions modulating lipid metabolism.^{52,53} We demonstrated that in *E3L.CETP* mice fed a HFD_{32%}, endothelial function was also significantly impaired after just 2 weeks of feeding in the AA but not in TA, as evidenced on paradoxical vasoconstriction in AA with preserved response to Ach in TA. Importantly, *E3L.CETP* mice exposed to a HFD_{32%} did not develop significant insulin resistance in contrast to *C57BL/6* HFD_{60%}-fed mice, indicating that early vascular dysfunction induced by HFD is not dependent on systemic insulin resistance. In the present study, mild insulin resistance was only observed in *E3L.CETP* female mice after 16 weeks of feeding with an HFD_{32%} but not after 2 weeks (H.M.G. Princen, PhD, et al, unpublished data, 2004). Moreover, even diets with a higher fat content (60 kcal% or 45 kcal%) induced systemic insulin resistance in *E3L.CETP* mice only after a longer period of feeding than 2 weeks.^{28,54,55} Similarly to HFD_{60%} in *C57BL/6*, *E3L.CETP* mice fed a HFD_{32%} did not display a lower nitrite plasma concentration despite significant impairment of endothelial function in the AA, pointing again to a local, not systemic nature of early-phase endothelial dysfunction in HFD-fed mice involving intercellular communication between endothelial cells and PVAT in the vessel wall in HFD-induced vascular pathology.⁵⁶

CONCLUSIONS

We demonstrated here that short-term feeding with a HFD in 2 different mouse models resulted in the impairment of the vascular response in the AA, whereas this response was largely preserved in the TA. The heterogeneous endothelial response was ascribed to distinct PVAT composition, including white adipose tissue-like characteristics in the AA and brown adipose tissue-like characteristics in the TA, but was not associated with systemic insulin resistance or with classical systemic biomarkers of endothelial dysfunction. These data underscore the notion that PVAT plays a fundamental role in the modulation of endothelial function in mouse models of metabolic syndrome and obesity, which could also be relevant to mechanisms of early endothelial dysfunction induced by fat load in humans.⁵⁷ Finally, our results also support the proposal that PVAT-targeted diagnosis^{58,59} and therapy^{60,61} might offer a novel approach to prevent residual vascular risks linked to the loss of PVAT-dependent homeostatic and vasoprotective function in response to excessive fat load, leading to endothelial dysfunction.^{62,63}

ARTICLE INFORMATION

Received April 21, 2020; accepted August 26, 2020.

Affiliations

From the Jagiellonian Centre for Experimental Therapeutics (JCET), Jagiellonian University, Krakow, Poland (A.B., A.K.-R., B.P., J.S.-P., K.C., B.M., K.M.-G., A.J., E.K., Z.M., A.K., A.K., M.W., S.C.); Chair of Pharmacology, Faculty of Medicine, Jagiellonian University Medical College (A.K.-R., B.M., S.C.) and Chair and Department of Toxicology, Faculty of Pharmacy (M.W.), Jagiellonian University Medical College, Krakow, Poland; Faculty of Chemistry, Jagiellonian University, Krakow, Poland (Z.M., A.K.); and Metabolic Health Research, Gaubius Laboratory, The Netherlands Organisation for Applied Scientific Research (TNO), Leiden, The Netherlands (E.J.P., H.M.P.).

Acknowledgments

The authors would like to thank Agnieszka Zakrzewska for expert technical assistance and measurements of nitrite and nitrate concentration in plasma, Zuzanna Kuryłowicz for help with immunohistochemical staining, and Krystyna Wandzel and Kristina Szczepanik for their excellent technical assistance in PWV measurements. Anna Kierońska-Rudek acknowledges the fellowship with the project No. POWR.03.02.00-00-1013/16. Anna Bar and Krzysztof Czamara acknowledge the START scholarship, awarded by the Foundation for Polish Science (Foundation for Polish Science, START2020 program).

Sources of Funding

This work was supported by Polish National Science Centre grant: OPUS No. 2018/29/B/NZ7/01684 and by Team Tech-Core Facility program of the FNP (Foundation for Polish Science) co-financed by the European Union under the European Regional Development Fund (project No. POIR.04.04.00-00-5CAC/17-00).

Disclosures

None.

Supplementary Material

Figures S1–S4

REFERENCES

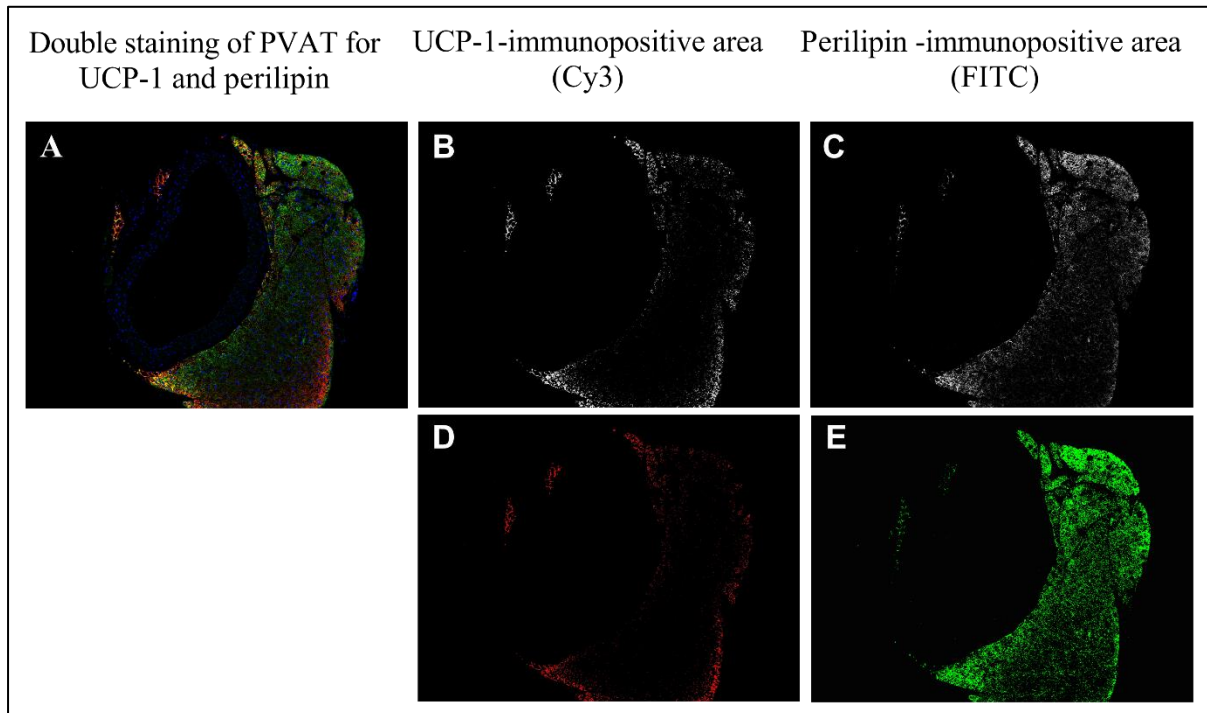
- McVeigh GE, Cohn JN. Endothelial dysfunction and the metabolic syndrome. *Curr Diab Rep*. 2003;3:87–92.
- Schachinger V, Britten MB, Zeiher AM. Prognostic impact of coronary vasodilator dysfunction on adverse long-term outcome of coronary heart disease. *Circulation*. 2000;101:1899–1906.
- Halcox JJP, Schenke WH, Zalos G, Mincemoyer R, Prasad A, Waclawiw MA, Nour KRA, Quyyumi AA. Prognostic value of coronary vascular endothelial dysfunction. *Circulation*. 2002;106:653–658.
- Csányi G, Gajda M, Franczyk-Zarow M, Kostogryz R, Gwoźdź P, Mateuszuk L, Sternak M, Wojcik L, Zalewska T, Walski M, et al. Functional alterations in endothelial NO, PGI₂ and EDHF pathways in aorta in ApoE/LDLR^{-/-} mice. *Prostaglandins Other Lipid Mediat*. 2012;98:107–115.
- Smeda M, Kieronska A, Adamski MG, Proniewski B, Sternak M, Mohaisen T, Przyborowski K, Derszniak K, Kaczor D, Stojak M, et al. Nitric oxide deficiency and endothelial-mesenchymal transition of pulmonary endothelium in the progression of 4T1 metastatic breast cancer in mice. *Breast Cancer Res*. 2018;20:86.
- Chlopicki S, Nilsson H, Mulvany MJ. Initial and sustained phases of myogenic response of rat mesenteric small arteries. *Am J Physiol Heart Circ Physiol*. 2001;281:H2176–H2183.
- Gil-Ortega M, Somoza B, Huang Y, Gollasch M, Fernández-Alfonso MS. Regional differences in perivascular adipose tissue impacting vascular homeostasis. *Trends Endocrinol Metab*. 2015;26:367–375.
- Gollasch M, Dubrovskaya G. Paracrine role for perivascular adipose tissue in the regulation of arterial tone. *Trends Pharmacol Sci*. 2004;25:647–653.
- Eringa EC, Bakker W, Smulders YM, Serné EH, Yudkin JS, Stehouwer CD. Regulation of vascular function and insulin sensitivity by adipose tissue: focus on perivascular adipose tissue. *Microcirculation*. 2007;14:389–402.

10. Lohn M, Dubrovská G, Lauterbach B, Luft FC, Gollasch M, Sharma AM. Periadventitial fat releases a vascular relaxing factor. *FASEB J*. 2002;16:1057–1063.
11. Yu-Jing Gao YJ. Dual modulation of vascular function by perivascular adipose tissue and its potential correlation with adiposity/lipoatrophy-related vascular dysfunction. *Curr Pharm Des*. 2007;13:2185–2192.
12. Marchesi C, Ebrahimián T, Angulo O, Paradis P, Schiffrin EL. Endothelial nitric oxide synthase uncoupling and perivascular adipose oxidative stress and inflammation contribute to vascular dysfunction in a rodent model of metabolic syndrome. *Hypertension*. 2009;54:1384–1392.
13. Somoza B, Guzmán R, Cano V, Merino B, Ramos P, Díez-Fernández C, Fernández-Alfonso MS, Ruiz-Gayo M. Induction of cardiac uncoupling protein-2 expression and adenosine 5'-monophosphate-activated protein kinase phosphorylation during early states of diet-induced obesity in mice. *Endocrinology*. 2007;148:924–931.
14. Greenstein AS, Khavandi K, Withers SB, Sonoyama K, Clancy O, Jeziorska M, Laing I, Yates AP, Pemberton PW, Malik RA, et al. Local inflammation and hypoxia abolish the protective anticontractile properties of perivascular fat in obese patients. *Circulation*. 2009;119:1661–1670.
15. Henrichot E, Juge-Aubry CE, Pernin A, Pache JC, Velebit V, Dayer JM, Meda P, Chizzolini C, Meier CA. Production of chemokines by perivascular adipose tissue. *Arterioscler Thromb Vasc Biol*. 2005;25:2594–2599.
16. Bogaert YE, Linares S. The role of obesity in the pathogenesis of hypertension. *Nat Clin Pract Nephrol*. 2009;5:101–111.
17. Xia N, Horke S, Habermeier A, Closs EI, Reifensberg G, Gericke A, Mikhed Y, Münzel T, Daiber A, Förstermann U, et al. Uncoupling of endothelial nitric oxide synthase in perivascular adipose tissue of diet-induced obese mice. *Arterioscler Thromb Vasc Biol*. 2016;36:78–85.
18. Wang H, Luo W, Wang J, Guo C, Wang X, Wolffe SL, Bodary PF, Eitzman DT. Obesity-induced endothelial dysfunction is prevented by deficiency of P-selectin glycoprotein ligand-1. *Diabetes*. 2012;61:3219–3227.
19. Gil-Ortega M, Stucchi P, Guzmán-Ruiz R, Cano V, Arribas S, González MC, Ruiz-Gayo M, Fernández-Alfonso MS, Somoza B. Adaptive nitric oxide overproduction in perivascular adipose tissue during early diet-induced obesity. *Endocrinology*. 2010;151:3299–3306.
20. Ketonen J, Shi J, Martonen E, Mervaala E. Periadventitial adipose tissue promotes endothelial dysfunction via oxidative stress in diet-induced obese C57Bl/6 mice. *Circ J*. 2010;74:1479–1487.
21. Kobayashi R, Akamine EH, Davel AP, Rodrigues MA, Carvalho CR, Rossoni LV. Oxidative stress and inflammatory mediators contribute to endothelial dysfunction in high-fat diet-induced obesity in mice. *J Hypertens*. 2010;28:2111–2119.
22. Fitzgibbons TP, Kogan S, Aouadi M, Hendricks GM, Straubhaar J, Czech MP. Similarity of mouse perivascular and brown adipose tissues and their resistance to diet-induced inflammation. *Am J Physiol Heart Circ Physiol*. 2011;301:H1425–H1437.
23. Police SB, Thatcher SE, Charnigo R, Daugherty A, Cassis LA. Obesity promotes inflammation in periaortic adipose tissue and angiotensin II-induced abdominal aortic aneurysm formation. *Arterioscler Thromb Vasc Biol*. 2009;29:1458–1464.
24. Padilla J, Jenkins NT, Vieira-Potter VJ, Laughlin MH. Divergent phenotype of rat thoracic and abdominal perivascular adipose tissues. *Am J Physiol Regul Integr Comp Physiol*. 2013;304:R543–R552.
25. Bar A, Skorka T, Jasinski K, Sternak M, Bartel Ž, Tyrankiewicz U, Chlopicki S. Retrospectively-gated MRI for in vivo assessment of endothelium-dependent vasodilatation and endothelial permeability in murine models of endothelial dysfunction. *NMR Biomed*. 2016;29:1088.
26. Suraj J, Kurpińska A, Sternak M, Smolik M, Niedzielska-Andres E, Zakrzewska A, Chlopicki S, Walczak M. Quantitative measurement of selected protein biomarkers of endothelial dysfunction by micro-liquid chromatography-tandem mass spectrometry based on stable isotope dilution method. *Talanta*. 2019;194:1005–1016.
27. Westerterp M, Van Der Hoogt CC, De Haan W, Offerman EH, Dallinga-Thie GM, Jukema JW, Havekes LM, Rensen PC. Cholesteryl ester transfer protein decreases high-density lipoprotein and severely aggravates atherosclerosis in APOE*3-Leiden mice. *Arterioscler Thromb Vasc Biol*. 2006;26:2552–2559.
28. van den Hoek AM, van der Hoorn JWA, Maas AC, van den Hoogen RM, van Nieuwkoop A, Droog S, Offerman EH, Pieterman EJ, Havekes LM, Princen HMG. APOE*3Leiden.CETP transgenic mice as model for pharmaceutical treatment of the metabolic syndrome. *Diabetes Obes Metab*. 2014;16:537–544.
29. Sternak M, Bar A, Adamski MG, Mohaisen T, Marczyk B, Kieronska A, Stojak M, Kus K, Tarjus A, Jaisser F, et al. The deletion of endothelial sodium channel α (eNaC) impairs endothelium-dependent vasodilation and endothelial barrier integrity in endotoxemia in vivo. *Front Pharmacol*. 2018;9:178.
30. Bar A, Targosz-Korecka M, Suraj J, Proniewski B, Jaształ A, Marczyk B, Sternak M, Przybyto M, Kurpińska A, Walczak M, et al. Degradation of glycocalyx and multiple manifestations of endothelial dysfunction coincide in the early phase of endothelial dysfunction before atherosclerotic plaque development in apolipoprotein E/low-density lipoprotein receptor-deficient mice. *J Am Heart Assoc*. 2019;8:e011171. DOI: 10.1161/JAHA.118.011171.
31. Hartley CJ, Taffet GE, Michael LH, Pham TT, Entman ML. Noninvasive determination of pulse-wave velocity in mice. *Am J Physiol*. 1997;273:H494–H500.
32. Asmar R, Benetos A, Topouchian J, Laurent P, Pannier B, Brisac AM, Target R, Levy BI. Assessment of arterial distensibility by automatic pulse wave velocity measurement. Validation and clinical application studies. *Hypertension*. 1995;26:485–490.
33. Czamara K, Majka Z, Fus A, Matjasik K, Pacia MZ, Sternak M, Chlopicki S, Kaczor A. Raman spectroscopy as a novel tool for fast characterization of the chemical composition of perivascular adipose tissue. *Analyst*. 2018;143:5999–6005.
34. Przyborowski K, Proniewski B, Czarny J, Smeda M, Sitek B, Zakrzewska A, Zoladz JA, Chlopicki S. Vascular nitric oxide-superoxide balance and thrombus formation after acute exercise. *Med Sci Sports Exerc*. 2018;50:1405–1412.
35. Depre C, Havaux X, Renkin J, Vanoverschelde JL, Wijns W. Expression of inducible nitric oxide synthase in human coronary atherosclerotic plaque. *Cardiovasc Res*. 1999;41:465–472.
36. Proniewski B, Kij A, Sitek B, Kelley EE, Chlopicki S. Multiorgan development of oxidative and nitrosative stress in LPS-Induced Endotoxemia In C57Bl/6 mice: DHE-based in vivo approach. *Oxid Med Cell Longev*. 2019;2019:1–11.
37. Hempe JM, Ory-Ascani J. Simultaneous analysis of reduced glutathione and glutathione disulfide by capillary zone electrophoresis. *Electrophoresis*. 2014;35:967–971.
38. Suraj J, Kurpińska A, Olkiewicz M, Niedzielska-Andres E, Smolik M, Zakrzewska A, Jaształ A, Sitek B, Chlopicki S, Walczak M. Development, validation and application of a micro-liquid chromatography-tandem mass spectrometry based method for simultaneous quantification of selected protein biomarkers of endothelial dysfunction in murine plasma. *J Pharm Biomed Anal*. 2018;149:465–474.
39. Suraj J, Kurpińska A, Zakrzewska A, Sternak M, Stojak M, Jaształ A, Walczak M, Chlopicki S. Early and late endothelial response in breast cancer metastasis in mice: simultaneous quantification of endothelial biomarkers using mass spectrometry-based method. *Dis Model Mech*. 2019;12:dmm036269.
40. Walczak M, Suraj J, Kus K, Kij A, Zakrzewska A, Chlopicki S. Towards a comprehensive endothelial biomarkers profiling and endothelium-guided pharmacotherapy. *Pharmacol Rep*. 2015;67:771–777.
41. Czamara K, Majzner K, Pacia MZ, Kochan K, Kaczor A, Baranska M. Raman spectroscopy of lipids: a review. *J Raman Spectrosc*. 2015;46:4–20.
42. Targosz-Korecka M, Jaglarz M, Malek-Zietek KE, Gregorius A, Zakrzewska A, Sitek B, Rajfur Z, Chlopicki S, Szymonski M. AFM-based detection of glycocalyx degradation and endothelial stiffening in the db/db mouse model of diabetes. *Sci Rep*. 2017;7:15951.
43. Bar A, Kuś K, Manterys A, Proniewski B, Sternak M, Przyborowski K, Moorlag M, Sitek B, Marczyk B, Jaształ A, et al. Vitamin K2-MK-7 improves nitric oxide-dependent endothelial function in ApoE/LDLR-/- mice. *Vascul Pharmacol*. 2019;122-123:106581.
44. Arancibia-Radich J, González-Blázquez R, Alcalá M, Martín-Ramos M, Viana M, Arribas S, Delporte C, Fernández-Alfonso MS, Somoza B, Gil-Ortega M. Beneficial effects of murtilla extract and madecassic acid on insulin sensitivity and endothelial function in a model of diet-induced obesity. *Sci Rep*. 2019;9:599.
45. Liu JT, Song E, Xu A, Berger T, Mak TW, Tse HF, Law IK, Huang B, Liang Y, Vanhoutte PM, et al. Lipocalin-2 deficiency prevents endothelial dysfunction associated with dietary obesity: role of cytochrome P450 2C inhibition. *Br J Pharmacol*. 2012;165:520–531.
46. Grandl G, Straub L, Rudiger C, Arnold M, Wueest S, Konrad D, Wolfrum C. Short-term feeding of a ketogenic diet induces more severe

- hepatic insulin resistance than an obesogenic high-fat diet. *J Physiol*. 2018;596:4597–4609.
47. Czamara K, Majka Z, Sternak M, Koziol M, Kostogrys RB, Chlopicki S, Kaczor A. Distinct chemical changes in abdominal but not in thoracic aorta upon atherosclerosis studied using fiber optic raman spectroscopy. *Int J Mol Sci*. 2020;21:1–14.
 48. Ouchi N, Parker JL, Lugus JJ, Walsh K. Adipokines in inflammation and metabolic disease. *Nat Rev Immunol*. 2011;11:85–97.
 49. Chang L, Villacorta L, Li R, Hamblin M, Xu W, Dou C, Zhang J, Wu J, Zeng R, Chen YE. Loss of perivascular adipose tissue on peroxisome proliferator-activated receptor- γ deletion in smooth muscle cells impairs intravascular thermoregulation and enhances atherosclerosis. *Circulation*. 2012;126:1067–1078.
 50. van den Maagdenberg AM, Hofker MH, Krimpenfort PJ, de Bruijn I, van Vlijmen B, van der Boom H, Havekes LM, Frants RR. Transgenic mice carrying the apolipoprotein-E3-Leiden gene exhibit hyperlipoproteinemia. *J Biol Chem*. 1993;268:10540–10545.
 51. Princen HM, Pouwer MG, Pieterman EJ. Comment on “Hypercholesterolemia with consumption of PFOA-laced Western diets is dependent on strain and sex of mice” by Rebholz S.L. et al. *Toxicol Rep*. 2016 (3) 46–54. *Toxicol Rep*. 2016;3:306–309.
 52. Zadelaar S, Kleemann R, Verschuren L, De Vries-Van Der Weij J, Van Der Hoorn J, Princen HM, Kooistra T. Mouse models for atherosclerosis and pharmaceutical modifiers. *Arterioscler Thromb Vasc Biol*. 2007;27:1706–1721.
 53. Kühnast S, Fiocco M, Van Der Hoorn JW, Princen HM, Jukema JW. Innovative pharmaceutical interventions in cardiovascular disease: focusing on the contribution of non-HDL-C/LDL-C-lowering versus HDL-C-raising: a systematic review and meta-analysis of relevant preclinical studies and clinical trials. *Eur J Pharmacol*. 2015;763:48–63.
 54. Kleemann R, Van Erk M, Verschuren L, Van Den Hoek AM, Koek M, Wielinga PY, Jie A, Pellis L, Bobeldijk-Pastorova I, Kelder T, et al. Time-resolved and tissue-specific systems analysis of the pathogenesis of insulin resistance. *PLoS One*. 2010;5:e8817.
 55. Zadelaar AS, Boesten LS, Jukema JW, Van Vlijmen BJ, Kooistra T, Emeis JJ, Lundholm E, Camejo G, Havekes LM. Dual PPAR α/γ agonist tesaglitazar reduces atherosclerosis in insulin-resistant and hypercholesterolemic ApoE*3Leiden mice. *Arterioscler Thromb Vasc Biol*. 2006;26:2560–2566.
 56. da Costa RM, Fais RS, Dechandt CR, Louzada-Junior P, Alberici LC, Lobato NS, Tostes RC. Increased mitochondrial ROS generation mediates the loss of the anti-contractile effects of perivascular adipose tissue in high-fat diet obese mice. *Br J Pharmacol*. 2017;174:3527.
 57. Westphal S, Taneva E, Kästner S, Martens-Lobenhoffer J, Bode-Böger S, Kropf S, Dierkes J, Luley C. Endothelial dysfunction induced by postprandial lipemia is neutralized by addition of proteins to the fatty meal. *Atherosclerosis*. 2006;185:313–319.
 58. Antoniadou C, Shirodaria C. Detecting coronary inflammation with perivascular fat attenuation imaging. *JACC Cardiovasc Imaging*. 2019;12:201.
 59. Antoniadou C, Kotanidis CP, Berman DS. State-of-the-art review article. Atherosclerosis affecting fat: what can we learn by imaging perivascular adipose tissue? *J Cardiovasc Comput Tomogr*. 2019;13:288.
 60. van Dam AD, Boon MR, Berbée JFP, Rensen PCN, van Harmelen V. Targeting white, brown and perivascular adipose tissue in atherosclerosis development. *Eur J Pharmacol*. 2017;816:82–92.
 61. Hoeke G, Kooijman S, Boon MR, Rensen PC, Berbée JF. Role of brown fat in lipoprotein metabolism and atherosclerosis. *Circ Res*. 2016;118:173–182.
 62. Bhattacharjee R, Alotaibi WH, Kheirandish-Gozal L, Capdevila OS, Gozal D. Endothelial dysfunction in obese non-hypertensive children without evidence of sleep disordered breathing. *BMC Pediatr*. 2010;10:8.
 63. Jiménez MV, Estepa RM, Camacho RM, Estrada RC, Luna FG, Guitarte FB. Endothelial dysfunction is related to insulin resistance and inflammatory biomarker levels in obese prepubertal children. *Eur J Endocrinol*. 2007;156:497–502.

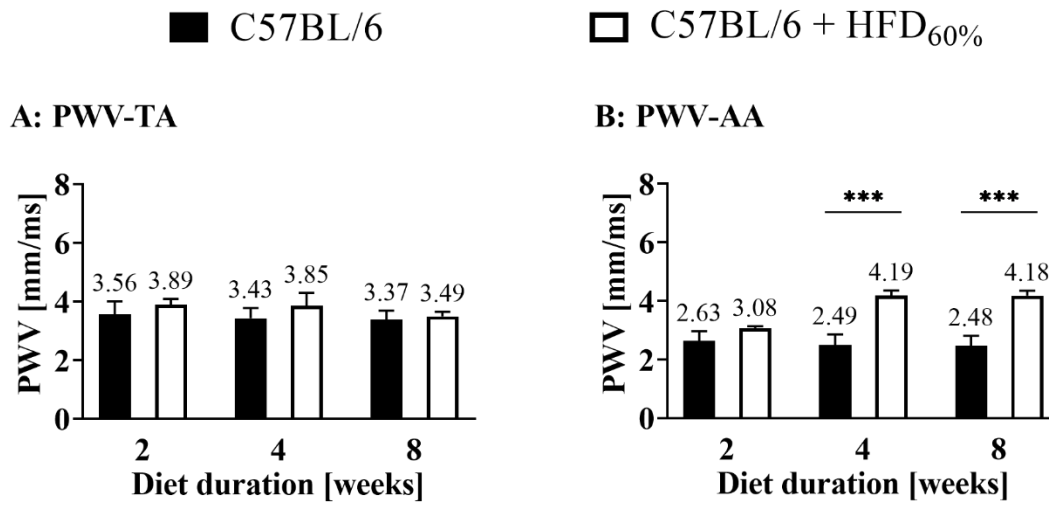
SUPPLEMENTAL MATERIAL

Figure S1. Algorithm for assessment of brown and white adipose tissue content in perivascular adipose tissue of thoracic and abdominal aorta.



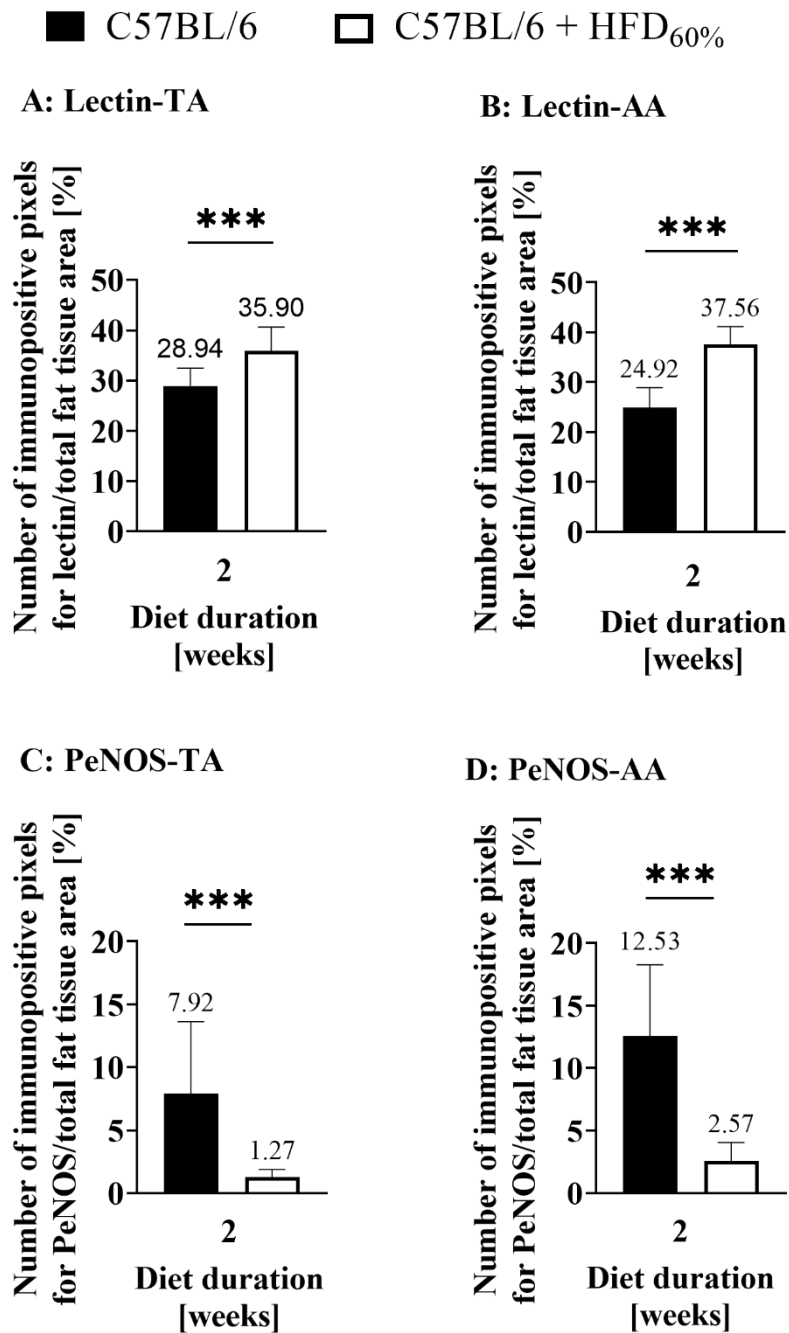
The representative images of aorta cross-section with perivascular adipose tissue (PVAT) simultaneously stained for UCP-1 and perilipin (A). Separation of the channels for Cy3-based immunofluorescence of UCP-1 and FITC-based immunofluorescence of perilipin are shown in (B) and (C) respectively. For quantitative analysis, the images of cross-section of PVAT were segmented in Ilastik software to assess the ratio of brown adipose tissue (BAT) to total fat tissue area. The result of an Ilastik segmentation are shown in (D,E). Red (D) indicates BAT (UCP-1 positive area) while green (E) indicates WAT (perilipin positive area) and both corresponds directly to the immunopositive pixels in respective channels. The number of pixels representing UCP-1 and perylipin were counted using ImageJ software. The results were expressed as the ratio of brown adipose tissue area (number of UPC-1 immunopositive pixels) to the total adipose tissue area (sum of UCP-1+ perylipim immunopositive pixels), and normalized to the respective control.

Figure S2. Effects of high-fat diet (HFD_{60%}) feeding on arterial stiffness measured as pulse wave velocity (PWV).



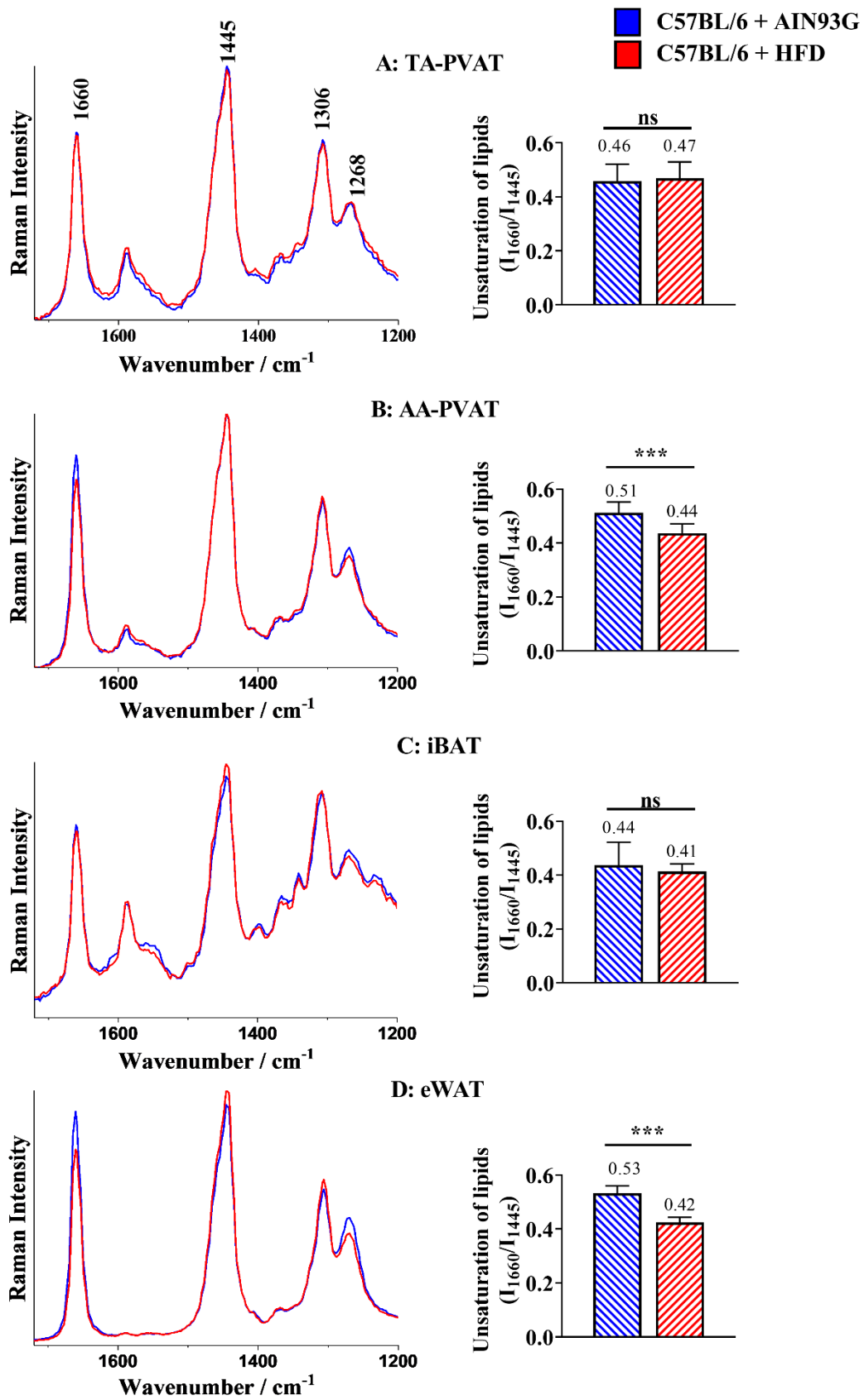
Pulse wave velocity (PWV) in the thoracic (TA, **A**) and the abdominal (AA, **B**) aorta in *C57BL/6* mice fed a high-fat diet (HFD_{60%}, white columns) for 2 (n=6, A; n=5, B), 4 (n=9, A; n=8, B) and 8 (n=7) weeks in comparison to age-matched *C57BL/6* mice fed a control diet (black columns, after 2 (n=7), 4 (n=9) and 8 (n=7, B; n=6, A) weeks of feeding). Statistics: two-way ANOVA followed by Tukey's post hoc test (normality was assessed using the Shapiro-Wilk test): ns - not statistically significant * $p < 0.05$, ** $p < 0.01$, *** $p < 0.001$.

Figure S3. Effects of high-fat diet (HFD_{60%}) feeding on adipose tissue immunohistochemical characteristics.



Ratio of immunopositive pixels for lectin (A, B) and phosphorylated endothelial nitric oxide synthase (PeNOS, C, D) to total adipose tissue area in the thoracic (A, C) and the abdominal aorta (B, D) in *C57BL/6* mice fed a high-fat diet (HFD_{60%}, white columns) for 2 weeks (n=17, A; n=15, B; n=14, C; n=13, D) in comparison to age-matched *C57BL/6* mice fed a control diet (black columns, n=18, D; n=17, A; n=15, B; n=14, C). Statistics: two-way ANOVA followed by Tukey's post hoc test (normality was assessed using the Shapiro-Wilk test): ns - not statistically significant * $p < 0.05$, ** $p < 0.01$, *** $p < 0.001$.

Figure S4. Effects of high-fat diet (HFD_{60%}) feeding on adipose tissue chemical characteristics.



Averaged Raman spectra and analysis of the lipid unsaturation degree (I_{1660}/I_{1444}) of the thoracic perivascular adipose tissue (**A**: TA-PVAT), abdominal perivascular adipose tissue (**B**: AA-PVAT), interscapular (**C**: iBAT) and epididymal adipose tissue (**D**: eWAT) in *C57BL/6* mice fed a HFD_{60%} for 4 weeks (red columns and lines; n=5) in comparison to age-matched *C57BL/6* mice fed a control diet (blue columns and lines, n=5). Statistics: Student's t-test (normality was assessed using the Shapiro-Wilk test): ns - not statistically significant * $p<0.05$, ** $p<0.01$, *** $p<0.001$.